JOURNAL OF AGRICULTURAL AND FOOD CHEMISTRY

pubs.acs.org/JAFC Article

A Novel Dry-Cured Ham Broth-Derived Peptide JHBp2 Effectively Inhibits *Salmonella typhimurium* In Vitro: Integrated Metabolomic, Proteomic, and Molecular Simulation Analyses

Ziyi Yang, Zixu Wang, Ruoxin Wang, and Wangang Zhang*

Cite This: *J. Agric. Food Chem.* 2024, 72, 14433−14447 Read Online

ACCESS | Metrics & More | Article Recommendations | Supporting Information

ABSTRACT: JHBp2 is a peptide purified from Jinhua ham broth with antibacterial activity against *Salmonella typhimurium*. Untargeted metabolomics and label-free quantitative proteomics were used to analyze metabolic and protein expression changes in *S. typhimurium* after JHBp2 treatment. Cell wall and membrane damage results indicate that JHBp2 has membrane-disruptive properties, causing leakage of intracellular nucleic acids and proteins. Metabolomics revealed 516 differentially expressed metabolites, involving cofactor biosynthesis, purine metabolism, ABC transporters, glutathione metabolism, pyrimidine metabolism, etc. Proteomics detected 735 differentially expressed proteins, involving pyruvate metabolism, amino acid biosynthesis, purine metabolism, carbon metabolism, glycolysis/gluconeogenesis, etc. RT-qPCR and proteomics results showed a positive correlation, and molecular docking demonstrated stable binding of JHBp2 to some differentially expressed proteins. In summary, JHBp2 could disrupt the *S. typhimurium* cell wall and membrane structure, interfere with synthesis of membrane-related proteins, trigger intracellular substance leak, and reduce levels of enzymes and metabolites involved in energy metabolism, amino acid anabolism, and nucleotide anabolism.

KEYWORDS: *antibacterial peptide, untargeted metabolomics, label-free quantitation proteomics, RT-qPCR, molecular docking, antibacterial mechanism*

1. INTRODUCTION

Salmonella is a significant foodborne pathogen that can cause human diarrheal disease after consumption of contaminated water, animal products, and plant products. In 2022, the FoodNet of CDC identified that *Salmonella* had the second highest infection incidence among all pathogens.[1] This has garnered significant attention that the misuse of antibiotics leads to the development of *Salmonella* resistance.[2] In addition, adverse reactions caused by antibiotics can cause significant damage to various body parts, including gastrointestinal tract, skin, kidneys, and nervous system.[3] Therefore, it is imperative to search for safer and more reliable oral antibacterial substances or foods with antibacterial properties.

Antimicrobial peptides (AMPs) are short-chain peptides, either naturally produced by organisms or artificially synthesized with the capacity of damaging or killing effects on bacteria, fungi, viruses, and parasites.[4] Importantly, AMPs have a unique nonspecific membrane rupture mechanism.[5] This mechanism not only avoids the emergence of microbial resistance but also prevents normal cells from damaging the host. In particular, AMPs produced during food processing are more acceptable and promising because of their safe origins.[6]

The mechanism underlying the action of AMPs primarily involves their interaction with the cell membrane of bacteria and the disruption of the cell membrane structure.[7] Both Gram-negative and Gram-positive bacteria have extremely hydrophobic plasma membrane layers[8] characterized by the abundance of phosphatidylserine (PS), cardiolipin (CL), and phosphatidylglycerol (PG); notably, the heads of these phospholipid molecules are negatively charged.[9] Therefore, peptides with antimicrobial properties tend to carry some positive charge and display high amphiphilicity.[4] The positive charge of peptides leads to electrostatic interactions with the negative charge of the bacterial cell membrane, resulting in the formation of holes on the membrane. This disrupts the functionality of the cell membrane, ultimately causing cell death by lysis.[10] In addition, some AMPs also can affect bacterial DNA/RNA/protein synthesis and metabolism, thereby affecting bacterial cell growth and proliferation.[11]

The amino acid sequences of AMPs often contain a certain amount of positively charged alkaline amino acids (such as lysine and arginine).[12] The lysine content in animal-derived proteins was significantly higher than that in grains and vegetables, which allowed them to produce more positively charged peptides after aging or cooking.[13] Dry-cured ham has produced a large number of bioactive peptides through long-term fermentation,[14] some of which have been proven to have antioxidant,[15] anti-inflammatory,[16] and antilisterial[17] activities. Our previous studies have demonstrated that there was still a large amount of bioactive peptides in the cooked Jinhua ham broth.[18]

Received: February 19, 2024
Revised: June 3, 2024
Accepted: June 4, 2024
Published: June 12, 2024

Advances in molecular detection technology have facilitated the elucidation of the antimicrobial mechanisms encompassing both physical fields or chemical compounds.[19] Specifically, proteomics, metabolomics, and transcriptomics all serve as important tools to investigate antimicrobial mechanisms.[20] Currently, multiomics have been applied to investigate the bacteriostatic mechanisms as this approach has the capacity to elucidate changes in organisms from a broad perspective. Previous studies have used integrated metabolomic and transcriptomic analyses to illuminate the bacteriostatic mechanism of thyme herb and cinnamon essential oil. Their study highlighted that aminoacyl-tRNA biosynthesis was one of the critical pathways by which EO influenced the metabolism of *Salmonella typhimurium*.[21] Combining transcriptomics and proteomic to explore the effects of plantaricin on methicillin-resistant *S. aureus*, it was found that differential genes and differential proteins were mainly enriched in nucleotide and amino acid metabolism, biofilms, and the synthesis of secondary metabolites.[22] Similarly, Mironenka et al.[23] conducted integrated metabolomic and proteomic analyses to examine the effect of *Trichoderma harzianum* metabolites on the metabolism of *Fusarium*. Their findings revealed substantial changes in proteins and metabolites involved in carbohydrate metabolism and redox processes before and after treatment.

In our previous study, more than 1500 peptides have been identified in Jinhua ham broth.[18] After isolation and purification, the JHBp2 (IKKVVKQASEGP, IC_{50} = 0.125 mg/mL against *Salmonella typhimurium*) was identified and obtained with a high bacteriostatic activity. It was from glyceraldehyde-3-phosphate dehydrogenase in meat and was dissolved in broth. However, the mechanism of bacterial inhibition by JHBp2 remains unknown. In order to determine the precise target of JHBp2 and its specific effect on bacterial metabolism, we analyzed the intracellular metabolite changes and the up- and downregulation of protein expression in *Salmonella typhimurium* after treatment with this antibacterial peptide by using untargeted metabolomics and label-free quantitation(LFQ) proteomics. The current study verified the antibacterial activity of a newly discovered peptide, JHBp2, derived from Jinhua ham broth while revealing its growth inhibitory mechanisms against *Salmonella typhimurium* in vitro.

2. MATERIALS AND METHODS

2.1. Materials. *Salmonella typhimurium* (ATCC14028) was purchased from Mingzhou Biotechnology (Zhejiang, China). IKKVVKQASEGP (95% purity) was synthesized by China Peptides Co., Ltd. (Hubei, China). Luria−Bertani (LB) medium was purchased from Hepebio Biotechnology Co., Ltd. (Qingdao, China). Coomassie brilliant blue G-250 was purchased from Macklin Biochemical Co., Ltd. (Shanghai, China). Trypsin was purchased from Promega Biotech Co., Ltd. (Beijing, China). Acetonitrile, SDT, methanol, and formic acid were purchased from Millipore Corporation (MA, USA). Trichloroacetic acid, DTT, urea nitrogen, and tris were purchased from Sigma-Aldrich Inc. (WI, USA). TransZol reagent was purchased from TransGen Biotech Co., Ltd. (Beijing, China). The rRNA Removal kit was purchased from NEB Inc. (MA, USA). Fragmentation buffer was bought from Macklin Biochemical Co., Ltd. (Shanghai, China).

2.2. Determination of Minimum Inhibitory Concentration (MIC). The approach outlined by Ikeda et al.[24] was adapted with certain modifications. The JHBp2 was formulated into 6.4 μM/mL using sterile normal saline and filtered through 0.22 μm sterile filter membranes to remove bacteria. The *S. typhimurium* concentration was adjusted to 10^5 CFU/mL after two activations with sterilized LB medium. The 100 μL of peptide solution was added to the first-row flat bottom wells of a sterile polystyrene 96-well microtiter plate and diluted by a 2-fold gradient in other row wells, using sterile normal saline. Then, 100 μL of bacterial broth was added to the wells to adjust the concentration of the peptide solution to 3.2, 1.6, 0.8, 0.4, 0.2, 0.1, and 0.05 μM/mL, respectively. LB medium without *S. typhimurium* was used as a negative control, and 200 μL of bacterial broth was used as a positive control. Each concentration was repeated five times (n = 5). The lowest concentration that could completely inhibit the growth of *S. typhimurium* at 37 °C for 24 h was the MIC.

2.3. *S. typhimurium* Inhibition Curves. The growth curve assay was quantified using the methods by Du et al.[22] with some modifications. The *S. typhimurium* was activated twice with sterilized LB mediums. Then, 1 mL of bacterial solution was added to 100 mL of LB medium and shaken (180 rpm) at 37 °C to an optical density of 0.4 at 400 nm. Then, 1 mL of JHBp2 (final concentration corresponding to 1/4, 1/3, 1/2, 1, 3/2, or 2 MIC) or normal saline was added to bacterial solution with continuous shaking. The absorbance of samples was measured at 600 nm by a UV spectrophotometer (Spark2010014158, TECAN Austria GmbH, Grödig, Austria) every 30 min.

2.4. Cell Wall and Membrane Damage. *2.4.1. Surface Hydrophobicity of Bacterial Cells.* The surface hydrophobicity of the cell wall was quantified following methods described by Hou et al.[25] with some modifications. The *S. typhimurium* enrichment solution was centrifuged at 5000 g for 5 min and was washed twice by PBS. Then, the bacterial solution were resuspended to 10^8 CFU/mL in 0.1 M KNO3 and reacted with the JHBp2 (final concentration corresponding to 1/4, 1/3, 1/2, 1, 3/2, and 2 MIC) for 2 h at 37 °C. JHBP2 was replaced by physiological saline as a control. The absorbance values at 405 nm were measured as A_0. Then, 1.2 mL of bacterial solution was mixed with 0.2 mL of hexadecane on a vortex for 2 min and left to stand for 20 min to completely separate the water layer and organic layer. The absorbance values of the water layer in sample at 405 nm were measured as A_1. The surface hydrophobicity of bacterial cell walls is related to the percentage of microbial adhesion; therefore, the percentage of microbial adhesion can be used to reflect the changes in the surface hydrophobicity of bacterial cell walls. The percentage of *S. typhimurium* adhesion was calculated following the equation below:

$$\text{The percentage of } S.\ \text{typhimurium adhesion } (\%) = \left(1 - \frac{A_1}{A_0}\right) \times 100$$

where A_0 indicates the absorbance values at 405 nm of sample before adding hexadecane and A_1 indicates the absorbance values at 405 nm of the water layer in sample after adding hexadecane.

2.4.2. Bacterial Cell Nucleic Acid and Protein Leakage Measurement. Cell nucleic acid and protein leakage were quantified following methods described by Yang et al.[26] with some modifications. The *S. typhimurium* enrichment solution concentrations were adjusted to 10^5 CFU/mL and reacted with the peptide solution for 2 h at 37 °C before centrifugation at 5,000 g for 5 min. The concentrations of peptide in the mixed bacterial-peptide solutions were 1/2, 1/3, 1/4, 1/5, and 1/6 MIC, respectively. The absorbances at 260 and 280 nm of the supernatant were measured to detect the loss of nucleic acids and proteins. The blank group consisted of the peptide solution only, while the control group consisted of the bacterial solution only. Each concentration was repeated five times (n = 5). The leakage of cellular nucleic acid and protein was expressed as the change of absorbance (ΔA) at 260 and 280 nm:

$$\Delta A = A_{\text{sam(con)}} - A_{\text{bla}}$$

where A_{sam} indicates the absorbance values of mixture solution at 260 and 280 nm, A_{con} indicates the absorbance values of bacterial solution at 260 and 280 nm, and A_{bla} indicates the absorbance values of peptide solution at 260 and 280 nm.

2.4.3. Scanning Electron Microscope (SEM). The *S. typhimurium* enrichment solution concentrations were adjusted to 10^8 CFU/mL and reacted with the peptide solution (final concentration corresponding to 1/2, 1, and 2 MIC) for 6 h at 37 °C before centrifugation at 8000 g for 10 min. The bacterial precipitate was washed 3 times with PBS before 2.5% (v/v) glutaraldehyde was added to fix the cells. After 12 h,

https://doi.org/10.1021/acs.jafc.4c01531
J. Agric. Food Chem. 2024, 72, 14433−14447

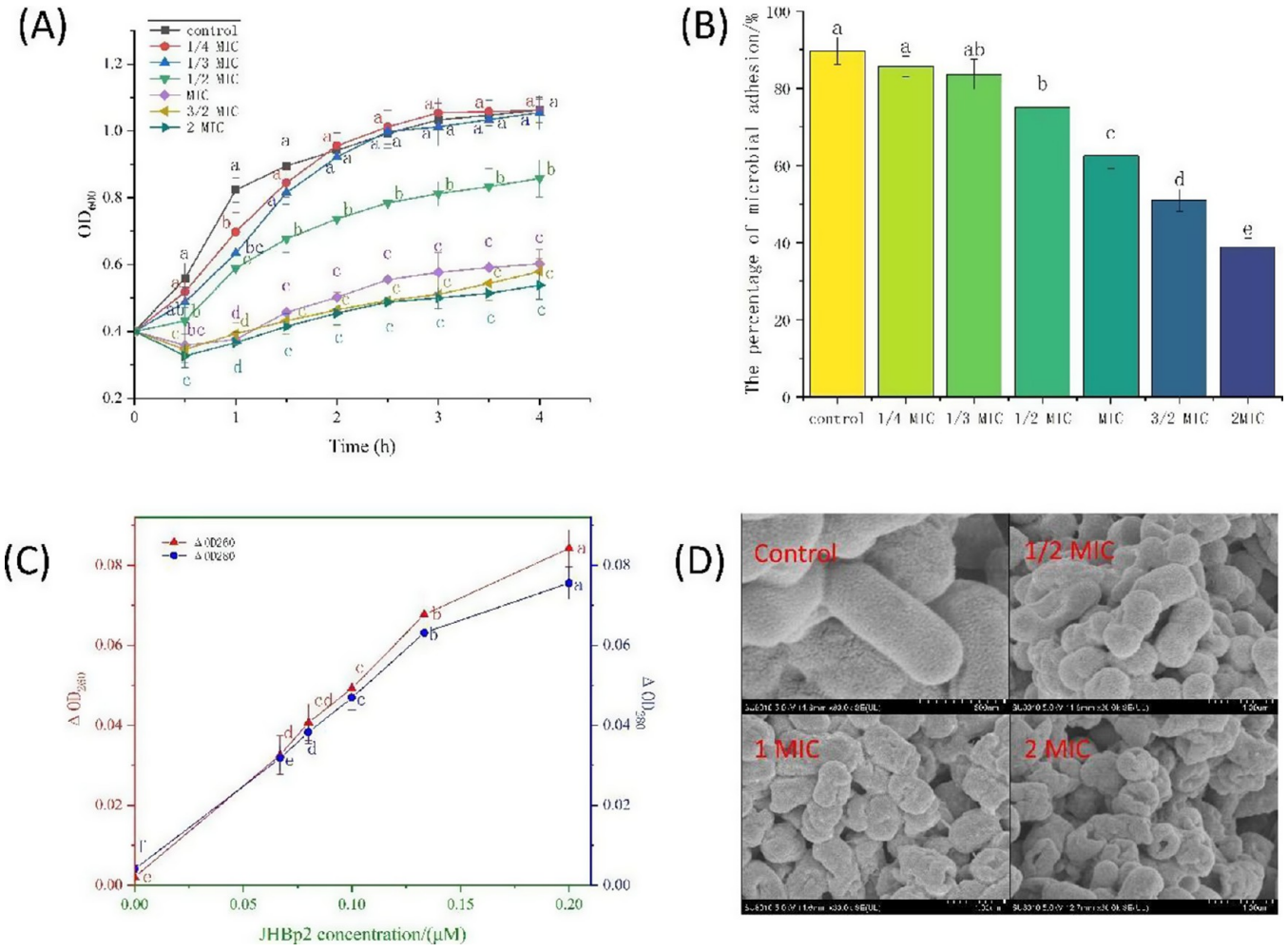

Figure 1. Destructive effect of JHBp2 on *Salmonella typhimurium* cell walls and membranes. (A) *S. typhimurium* inhibition curves, (B) surface hydrophobicity of bacterial cells, (C) bacterial cell nucleic acid and protein leakage, and (D) scanning electron microscope.

centrifugation and precipitate washing with PBS were repeated 3 times. 30, 50, 70, 80, 90, and 100% ethanols were sequentially used for dehydration, with each dehydration time of 10 min. The 100% ethanol was used for dehydration twice and for resuspension. The heavy suspension was dried on a sample loading platform and gold-plated. Finally, the sample was loaded and observed by using a scanning electron microscope (SU8010, Hitachi, Ltd., Japan).

2.5. Sample Preparation. The sub-MIC concentration was selected to treat bacteria.[27] The *S. typhimurium* concentration was adjusted to 1×10^5 CFU/mL after two activations. After incubation to logarithmic growth period, the wild-type (WT) group was added with sterile saline, and the AMP treatment (AMPT) group was added with 1/2 MIC of the JHBp2 (dissolved in sterile saline) and incubated together at 37 °C for 3 h to centrifugate and collect bacterial bodies.

2.6. Metabolomics Experiments. Metabolomics experiments were conducted in accordance with the methodologies established by Cheng et al.[28] with some modifications.

2.6.1. Metabolite Extraction. The samples from the AMPT and WT groups were taken and added to a 1:4 (v/v) mixture of ultrapure water and methanol. Cell fragmentation was performed using an ultrasonic system (Bioruptor, Diagenode Co., Ltd., Belgium). After cell fragmentation, the supernatants were freeze-dried after centrifugation, added to EP tubes containing tungsten beads, and ground at 65 Hz for 1 min. While the precipitates were added to 200 μL of SDT, the protein concentration was determined. The lyophilized supernatant was dissolved in 0.1 mL of a 1:4 (v/v) mixture of ultrapure water and methanol, and the supernatant was used for subsequent analysis after centrifugation. Equal amounts of the samples from the AMPT and WT groups were mixed to form a QC group for determining the stability of the system. The above procedures were repeated six times ($n = 6$).

2.6.2. UPLC−MS/MS Determination. The samples were separated by UPLC (Nexera X2 LC-30AD, Shimadzu Production Co., Ltd., Japan), and the ion fragments were detected with a mass spectrometer (QE Plus, Thermo Scientific, USA). Positive (+) and negative (−) ion fragments were collected separately and analyzed separately. MS data were preprocessed with MS-DIAL, and metabolites were identified by comparison with HMDB, MassBank public, and personal databases.

2.6.3. Bioinformatics Analysis. Multivariate statistical analysis was performed for metabolomics data using R software. KEGG (Kyoto Encyclopedia of Genes and Genomes) pathway analysis of differential metabolites between the AMPT and WT groups was performed using the online KEGG database.

2.7. Proteomics Experiments. *2.7.1. Protein Extraction.* The extraction of *S. typhimurium* protein was measured following methods described by Glatter et al.,[29] incorporating minor adaptations. The samples from AMPT and WT groups were added to the SDT lysis solution, and cells were broken using the ultrasonic system. After a boiling water bath at 100 °C for 3 min and ultrasonic crushing for 2 min, the supernatant was used for protein content after centrifugation, and electrophoresis (Mini-PROTEAN Tetra, Bio-Rad Laboratories, America) was utilized to verify the extraction effect. The extracted proteins were digested by trypsin, desalted, and lyophilized, and then, the lyophilized material was solubilized by adding 1 mL of 0.1% TFA. After centrifugation, the supernatant was extracted for the subsequent analysis, and the samples of AMPT and WT groups were mixed in equal

https://doi.org/10.1021/acs.jafc.4c01531
J. Agric. Food Chem. 2024, 72, 14433−14447

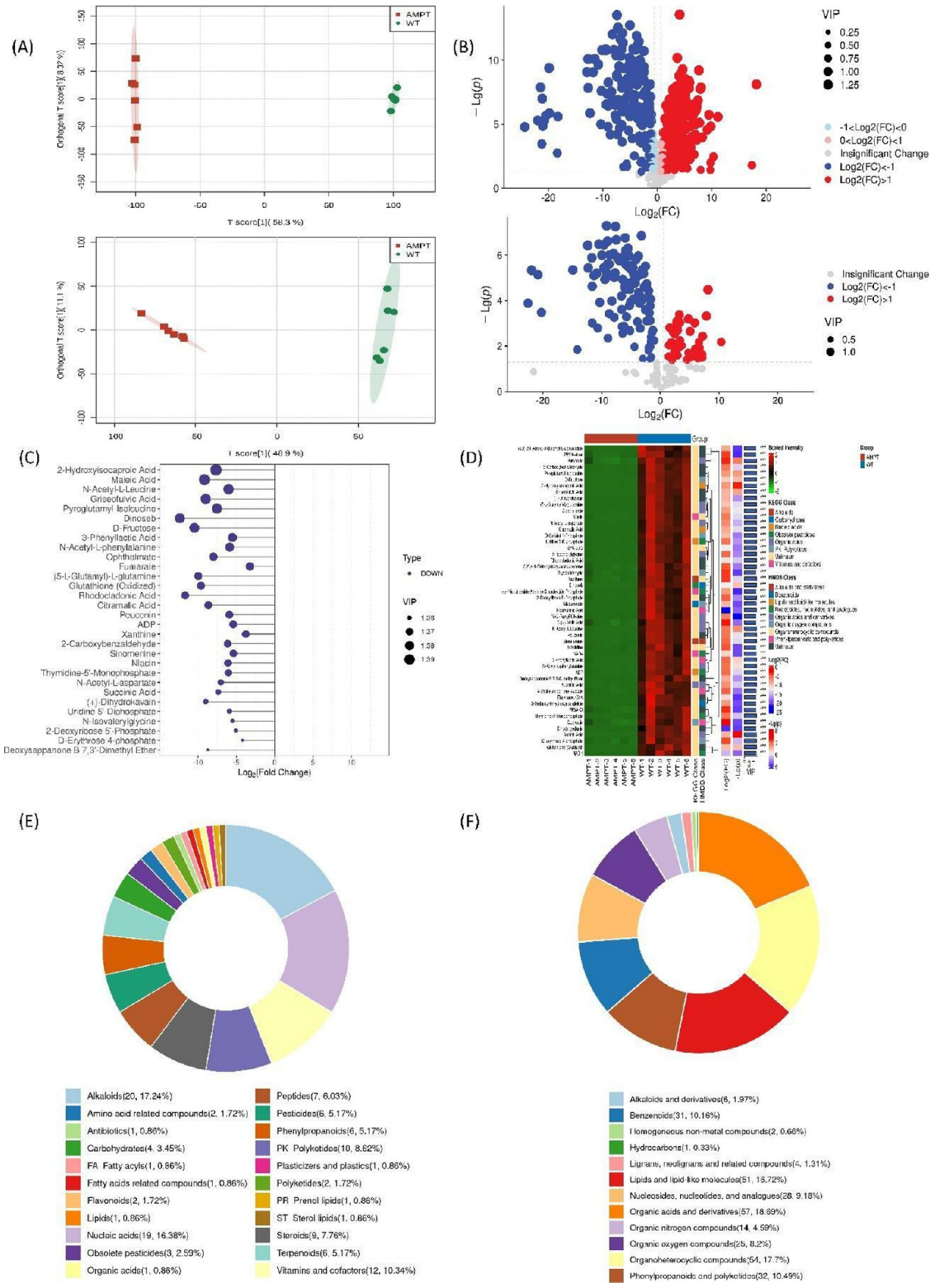

Figure 2. Differential metabolite screening and expression analysis. (A) Orthogonal partial least-squares discriminant analysis of cation and anion metabolites, (B) volcano map of differential cation and anion metabolites, (C) complex clustering heatmap of representative differential metabolites, (D) top 30 metabolites with the highest variable importance projection analysis, (E) KEGG enrichment classification loop diagram, and (F) HMDB enrichment classification loop diagram.

amounts to form a QC group for determining the system stability. The above process was repeated three times.

2.7.2. LC–MS/MS Determination. LC–MS/MS determination was measured following methods described by Yu et al.[30] with some modifications. The sample was separated by liquid chromatography (Easy-nLC1200, Thermo Scientific, America), and the peptide segments were identified by mass spectrometry. The results were analyzed using MSFragger[31] and the Uniprot-S. Typhimurium [90371]—144153, downloaded on February 22, 2023, was used as a

https://doi.org/10.1021/acs.jafc.4c01531
J. Agric. Food Chem. 2024, 72, 14433−14447

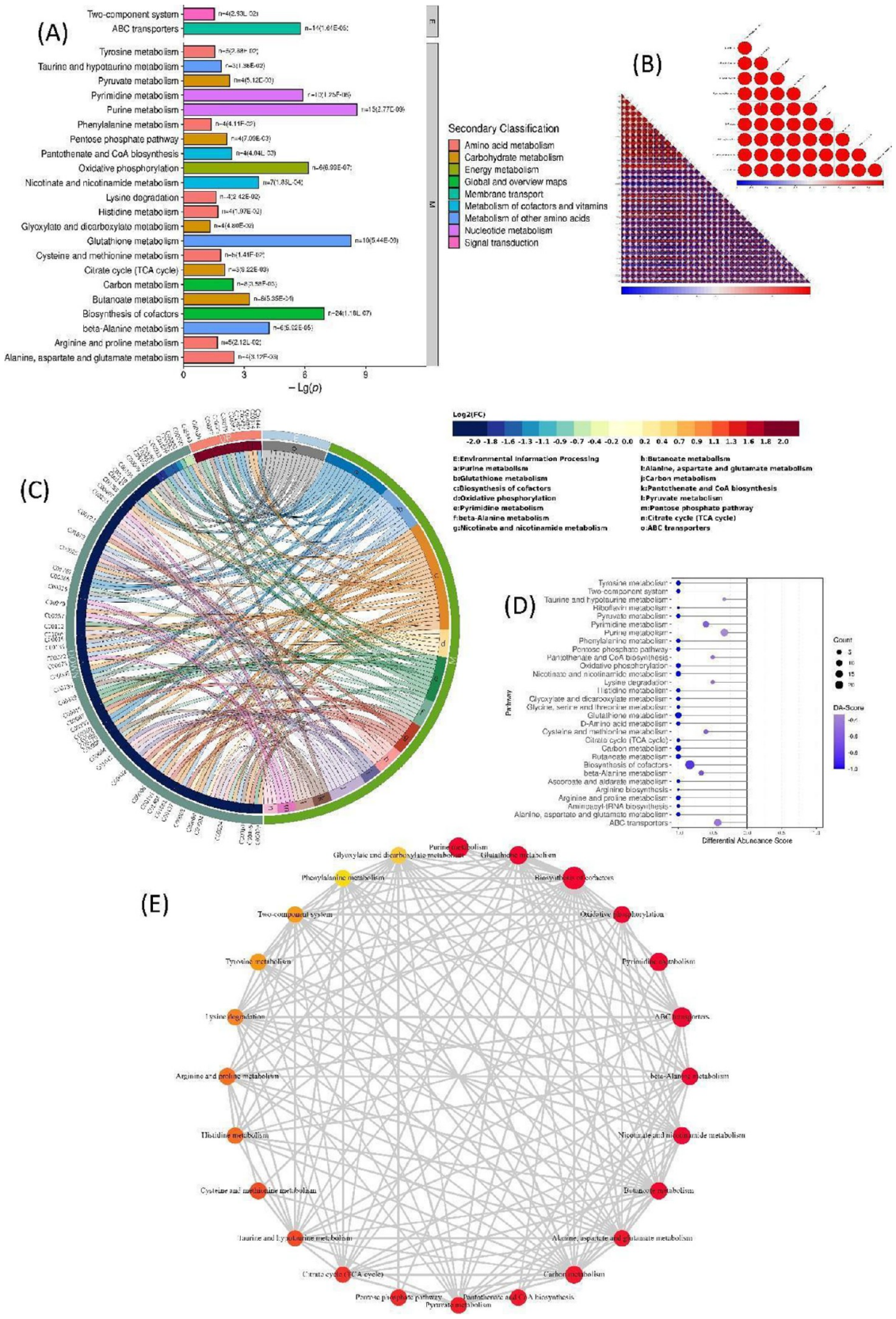

Figure 3. Functional analysis of differential metabolites. (A) KEGG pathway enrichment bar chart, (B) correlation analysis of differential metabolites, (C) string diagram of significant pathways and differential metabolites, (D) differential abundance score diagram of the pathways, and (E) pathway interaction diagram.

database for protein analysis. The MSFragger parameters were set according to Table S1.

2.7.3. Bioinformatics Analysis. Multivariate statistical analysis was performed for proteomics data by using R software. Gene ontology

https://doi.org/10.1021/acs.jafc.4c01531
J. Agric. Food Chem. 2024, 72, 14433−14447

(GO) and KEGG pathway analysis of differential proteomics between the AMPT and WT groups was performed.

2.8. Real-Time qPCR and Molecular Docking. Based on proteomics results, select 12 proteins, including yehZ, yiaO_1, pckA, deoC, gpmA, arcC, arcB, cpdB, yjjX, frr, trxA, and adhP, to validate by RT-qPCR. Total RNA was extracted using TransZol reagent according to the manufacturer's instructions using *S. typhimurium*, which was treated with 1/2 MIC JHBP2. The concentration and purity of total RNA were measured by using a spectrophotometer (NanoDrop 2000, Thermo Scientific, USA). First, rRNA was removed using rRNA Removal kits, and mRNA was fragmented using fragmentation buffers at 94 °C for 5 min. Then, random hexamers were used for reverse transcription. Finally, cDNA was mixed with the qPCR master mixture, and the mixture was analyzed by a real-time fluorescence quantitative PCR analysis system (PikoReal, Thermo Scientific, USA). The 16s rRNA housekeeping gene was used as an internal reference gene. The genes corresponding to 12 proteins (the sequences in Table S2) were analyzed using the $2^{-\Delta\Delta Ct}$ method.

The 3D structure of 12 proteins was constructed using Alpha Fold (https://alphafold.ebi.ac.uk/). By using RDKit[32] to call the Embed-Molecule function in the Chem. AllChem module and utilizing the Experimental Torsion Basic Knowledge Distance Geometry (ETKDG) algorithm function,[33] JHBP2 was generated into several peptide-based 3D conformations using the corrected distance geometry algorithm. The MMFFOptimizeMolecule module was then used to optimize the structure and energy of the small molecules with MMFF94 parameters.[34] The optimized JHBp2 was used as a ligand and docked with 12 proteins using smina software,[35] with an approximation of 80 (exhaustiveness). Each docking required the generation of 20 conformations. PyMOL 2.5.1[36] and PLIP[37] were used for visualization and chemical bond analysis.

2.9. Statistical Analysis. The data were analyzed by SAS software (SAS Company, NC, USA) depending on the one-way analysis of variance and Duncan's multiple range test. When $P < 0.05$, it was considered a significant difference. The results were presented as mean ± standard error.

3. RESULTS

3.1. Destructive Effect of JHBp2 on *S. typhimurium* Cell Walls and Membranes. As indicated in Table S3, when the JHBp2 concentration was higher than 0.4 μM/mL, there was no bacterial growth, so MIC_{JHBp2} = 0.4 μM/mL for *S. typhimurium*.

After treatment with 1, 3/2, and 2 MIC JHBp2, the OD_{600} of *S. typhimurium* decreased at 0.5 h and gradually increased afterward. The OD_{600} values of the remaining treatment groups consistently increased. On the one hand, there were no significant differences ($p > 0.05$) between the 1/4 and 1/3 MIC groups and the control group at 1.5−4 h. On the other hand, there were consistently significant differences ($p < 0.05$) between the 1/2, 1, 3/2, and 2 MIC groups and the control group. The degree of hydrophobicity of the bacterial surface determines the proportion of the bacteria that can adsorb to hexadecane (nonpolar solvent).[38] As shown in Figure 1B, when the concentration of JHBp2 ≥ MIC, the hydrophobicity of the cell surface was significantly reduced ($p < 0.05$) from 89.69% in the control group to 38.97% in the 2 MIC treatment, and the effect of JHBp2 on the hydrophobicity of the cell surface of the bacterium was concentration-dependent.

Alterations in cell membrane permeability can be reflected by the leakage of protein and nucleic acids.[26] The values of ΔOD_{260} and ΔOD_{280} increase when more intracellular nucleic acids and proteins escape into the supernatant.[39] As indicated in Figure 1C, JHBp2 had a strong destructive effect on the cell membranes of *S. typhimurium*, and JHBp2-induced leakage of nucleic acids and proteins was characterized in a dose-dependent manner. In the same way, the SEM (Figure 1D) showed that 1/2 MIC JHBp2 caused the *S. typhimurium* cell wall to concave compared to the control, while MIC and 2 MIC JHBp2 caused the bacteria to rupture.

3.2. Metabolomic Analysis. *3.2.1. Differential Metabolite Screening and Expression Analysis.* As shown in Figure 2A, whether in cation mode or anion mode, the orthogonal partial least-squares discriminant analysis (OPLS-DA) revealed that the metabolites of the AMPT group and the WT group had a large degree of separation. The metabolites of the WT group were grouped close to each other, indicating an enhanced biological reproducibility. As indicated in Figure 2B, 381 significant differential cation metabolites and 135 differential anion metabolites were identified between AMPT and WT groups based on the following screening criteria: fold-change (FC) > 1.5 or <0.667, $p < 0.05$, and variable importance projection (VIP) score >1. Of these, 212 were upregulated (red) and 169 were downregulated in the AMPT group (blue) as cation metabolites, while 29 were upregulated and 106 were downregulated in the AMPT group as anion metabolites.

Figure 2C shows the top 30 differential metabolites with the highest importance according to the VIP score. The top 10 metabolites with the highest VIP score were 2-hydroxyisocaproic acid, maleic acid, N-acetyl-L-leucine, griseofulvic acid, pyroglutamyl-lsoleucine, dinoseb, D-fructose, 3-phenyllactic acid, N-acetyl-lphenylalanine, and ophthalmate, which were all downregulated in the AMPT group.

Figure 2D shows the complex clustering heatmap of differential metabolites. The complex heatmap revealed that the top 50 highest VIP score differential metabolites of the AMPT group were all downregulated. Functional analyses of differential metabolites were performed using both KEGG enrichment (Figure 2E) and HMDB enrichment (Figure 2F). KEGG enrichment revealed that the differential metabolites were mainly alkaloids (17.24%), nucleic acids (16.38%), vitamins and cofactors (10.34%), PK polyketides (8.62%), steroids (7.76%), etc. Meanwhile, HMDB enrichment revealed that the differential metabolites mainly included organic acids and derivatives (18.69%), organoheterocyclic compounds (17.7%), lipids and lipid-like molecules (16.72%), phenylpropanoids, polyketides (10.49%), benzenoids (10.16%), etc.

3.2.2. Functional Analysis of Differential Metabolites. The 30 highest 30 KEGG pathways, according to *p*-values, were selected. The KEGG pathway enrichment classification (Figure 3A) indicated that these differential metabolites were mainly associated with global and overview amps ($n = 32$), nucleotide metabolism ($n = 27$), amino acid metabolism ($n = 26$), and carbohydrate metabolism ($n = 21$). Additionally, differential metabolites were enriched in two-component systems ($n = 4$) and ABC transporters ($n = 14$), involving signal transduction and membrane transport in secondary environmental information processing pathways.

As shown in Figure 3B, the correlation among the contents of the top 300 differential metabolites was examined. There was always a positive correlation between the differential metabolites in higher content. Among the 10 metabolites with the highest upregulation, the levels of metabolites all were positively correlated. The decrease in differential metabolite content increased the blue color intensity in the heatmap, indicating an increased negative correlation between differential metabolites.

Figure 3C shows the chord plots between the 15 significantly enriched pathways and the associated differential metabolites. Most differential metabolites were significantly downregulated. Only minority metabolites, such as GMP, vitamin B6, carnitine,

https://doi.org/10.1021/acs.jafc.4c01531
J. Agric. Food Chem. 2024, 72, 14433−14447

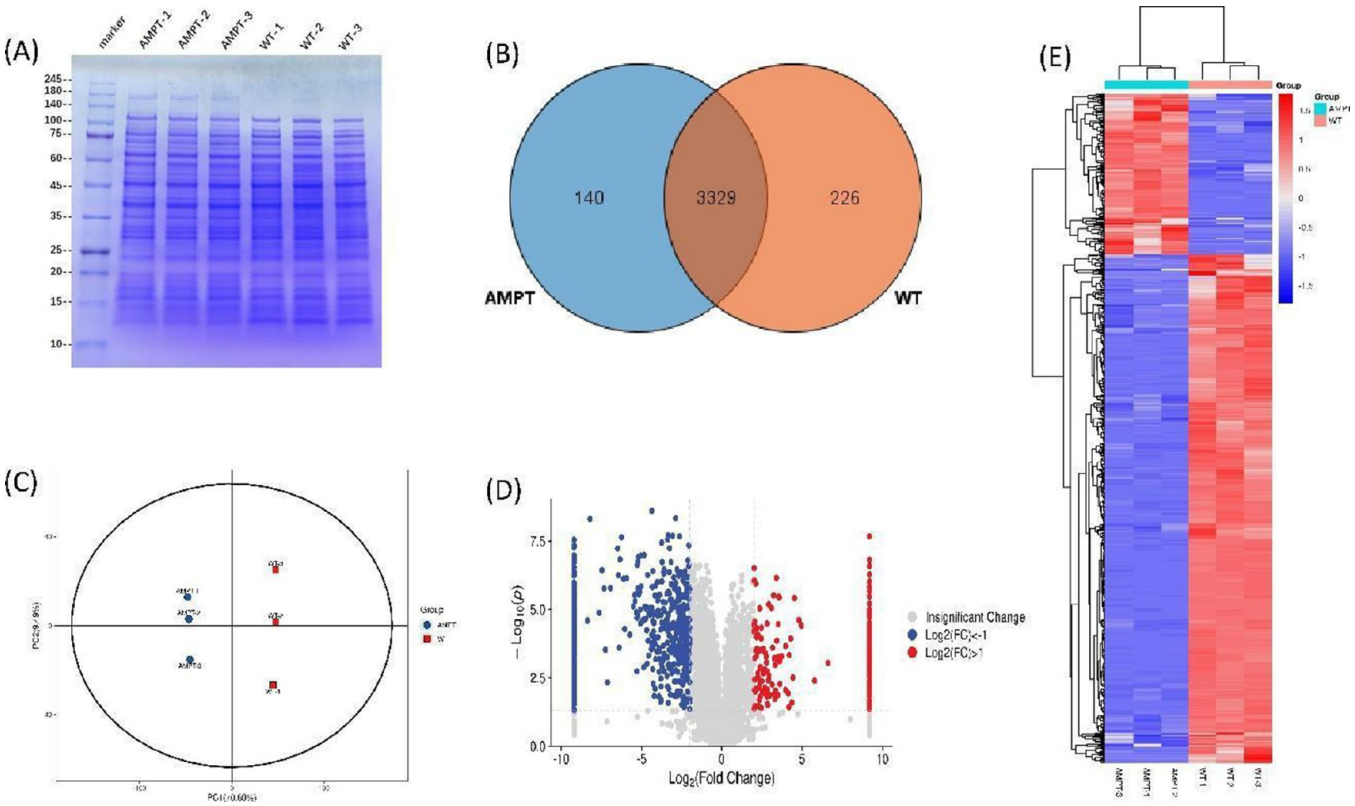

Figure 4. Differential proteins screening and expression analysis. (A) Sodium dodecyl sulfate-polyacrylamide gel electrophoresis, (B) Venn diagram of proteins in the AMPT and wild-type groups, (C) PCA score chart, (D) volcano chart of differential proteins, and (E) cluster analysis chart.

and vitamin K_1, were upregulated. The abundances of acetyl coenzyme A (n = 7), fumaric acid (n = 7), succinate (n = 7), glutamate (n = 6), 5,6-Dihydrouracil (n = 3), ADP (n = 3), NADP (C00006, n = 3), NAD (n = 3), etc., which were downregulated, were associated with more metabolic pathways. These metabolites were mainly associated with energy and amino acid metabolism. Each pathway involves multiple differential metabolites. Biosynthesis of cofactors (n = 24), purine metabolism (n = 15), ABC transporters (n = 14), glutathione metabolism (n = 10), pyrimidine metabolism (n = 10), carbon metabolism (n = 8), nicotinate and nicotinamide metabolism (n = 7), and butanoate metabolism (n = 6) involved more differential metabolites.

Furthermore, the effect of JHBp2 treatment on the differential abundance score (DA score) of metabolites was subjected to analysis. As shown in Figure 3D, all metabolic pathways were significantly downregulated with the biosynthesis of cofactors, purine metabolism, ABC transporters, glutathione metabolism, pyrimidine metabolism, and carbon metabolism pathway involving increased numbers of differential metabolites. The analysis of the generic interaction network (Figure 3E) revealed that these 6 metabolism pathways were also closely associated with other pathways.

3.3. Proteomic Analysis. *3.3.1. Differential Proteins Screening and Expression Analysis.* As shown in Table S4 and Figure 4A, the minimum amount of extracted protein was 1.18 mg, and clear bands were obtained without trailing after electrophoresis. As shown in Figure 4B, the WT and AMPT groups shared 3329 proteins and then haved 226 and 140 unique proteins, respectively. PCA (Figure 4C) revealed that the PC1 principal component accounted for 70.69%. The criteria to identify differential proteins were as follows: FC > 2 or 0 < FC < 0.5 and $p < 0.05$. As shown in Figure 4D, 735 proteins were significantly and differentially expressed (558 downregulated and 176 upregulated) between the AMPT and WT groups.

The heatmap of the cluster distribution (Figure 4E) indicated a clear distinction between the AMPT and WT groups with significant overall differences. The expression of proteins within the groups was significantly different, enabling further functional annotation analysis using the GO database.

3.3.2. Functional Analysis of Differential Proteins. Analysis of the subcellular localization of differential proteins (Figure 5A) revealed that most proteins were localized to the membrane (65.69%), followed by the cytoplasm (25.49%). The cell membrane and cytoplasm accounted for the localization of over 90% of the proteins. Additionally, some proteins were localized to the ribosomes (4.9%), extracellular regions (1.96%), cell wall (0.98%), and bacterial flagella (0.98%).

As shown in Figure 5B, GO analysis revealed that the differentially expressed proteins were primarily enriched in the following biological process (BP) categories: cellular processes (n = 258) and metabolic processes (n = 237). The other BP categories in which the differentially expressed proteins were enriched were localization (n = 72), biological regulation (n = 38), regulation of biological processes (n = 37), and response to stimulus (n = 21).

Further analysis of the secondary terms in the BP category (Figure 5C) revealed that the differential proteins were mainly involved in alkaloid metabolic processes (such as carnitine and betaine), amino acid metabolic processes (such as serine family amino acid, α-amino acid, and sulfur amino acid metabolism), energy metabolic pathways (such as glucose 6-phosphate synthesis/metabolism, NADPH regeneration, and NADP metabolic processes), oligosaccharide metabolic processes

https://doi.org/10.1021/acs.jafc.4c01531
J. Agric. Food Chem. 2024, 72, 14433−14447

Figure 5. Functional analysis of differential proteins. (A) Subcellular localization analysis of differential proteins, (B) gene ontology function note, (C) top 20 biological process categories, (D) top 20 cell component categories, (E) top 20 molecular function categories, (F) KEGG pathway enrichment bubble diagram, (G) enrichment butterfly diagram, and (H) pathway/protein interaction diagram.

(such as GDP-mannose biosynthesis), cellular catabolic metabolism, and nucleotide catabolism.

The limited numbers of proteins were enriched in cellular anatomical entity (n = 133) and protein-containing complexes (n = 15) in the CC term. Further analysis of the secondary terms

https://doi.org/10.1021/acs.jafc.4c01531
J. Agric. Food Chem. 2024, 72, 14433−14447

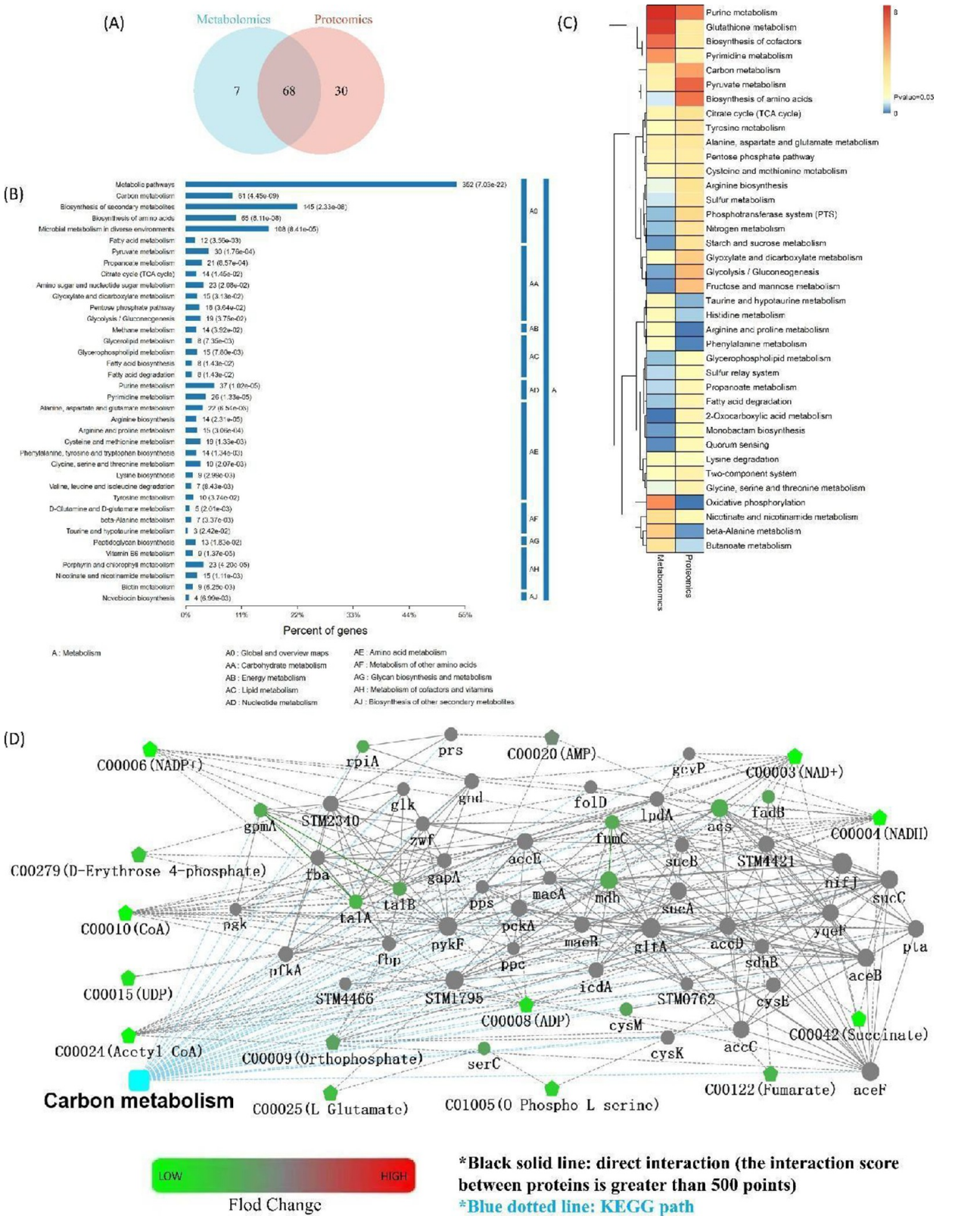

Figure 6. Correlation between metabolomic and proteomic analysis results: (A) KEGG pathways shared between the metabolome and proteome, (B) KEGG metabolic pathway enrichment, (C) *p*-value heatmap of shared KEGG pathways, and (D) carbon metabolism network diagram.

in the CC term (Figure 5D) revealed that the periplasmic space accounted for the highest enrichment, followed by the outer membrane-bound periplasmic space and bacterial micro-compartments. Additionally, the rest of the proteins in the top 10 proteins, enriched in CC term, were related to bacterial cell membranes, including plasma membrane protein complexes, ATPase-dependent transmembrane transport complexes, ABC transporter complexes, transmembrane transport protein

https://doi.org/10.1021/acs.jafc.4c01531
J. Agric. Food Chem. 2024, 72, 14433−14447

complexes, and intrinsic/integral components of membranes. Most of these proteins were transmembrane transporter proteins, largely determining the function of the bacterial cell membrane.[40] This is consistent with the results that JHBp2 treatment increased the bacterial cell wall and membrane permeability mentioned earlier.

In the MF term, the differential proteins were mainly enriched in catalytic activity (n = 278), binding (n = 161), transporter activity (n = 44), and transcriptional regulatory activity (n = 22). Further analysis of the secondary terms in the MF term (Figure 5E) revealed that the top seven proteins were related to cation binding and ion channel activities.

As indicated in Table S5, among the top 10 lowest FDR (False Discovery Rate) proteins, DUF2511 domain-containing protein (A0A0D6FPX9) belonged to the YebY family protein, carbamate kinase (A0A0D6HNW0, A0A3Y1BJM0) was involved in arginine biosynthesis and purine metabolism, ribosome-recycling factor (P66738) was involved in translation process, ornithine carbamoyltransferase (Q8ZK35) was involved in arginine biosynthesis, thioredoxin 1 (P0AA28) was involved in the metabolism of other amino acids, 2-iminobutanoate/2-iminopropanoate deaminase (Q7CP78, A0A701L0L9) was related to the generation of 2-aminoacylate (2AA), and alcohol dehydrogenase (A0A0F6B1I0) was involved in glycolysis/gluconeogenesis, fatty acid degradation, tyrosine metabolism, and pyruvate metabolism. In contrast, phosphatidylglycophorophosphatase A (A0A0F6AXP4) was involved in lipid metabolism.

The KEGG pathway analysis of differential proteins (Figure 5F) reveals that the differential proteins in AMPT were enriched in the cellular process pathway related to the flagellar assembly, bacterial chemotaxis, and quorum sensing of bacteria. In the environmental information processing pathway, the differential proteins were mainly related to the phosphotransferase system (PTS) and the two-component system. These proteins also play integral roles in various physiological processes, such as transport, regulation, signal transduction, and external stimulus response. Additionally, differential proteins were enriched in pathways related to cationic antimicrobial peptide (CAMP) resistance.

In the metabolic pathways, the involvement of differential proteins in pyruvate metabolism, amino acid biosynthesis, purine metabolism, carbon metabolism, and glycolysis/gluconeogenesis has widely varied. Among the 12 significantly downregulated pathways (Figure 5G), 6 (50%) energy metabolism-related pathways were pyruvate metabolism, carbon metabolism, glycolysis/gluconeogenesis, dicarboxylic acid metabolism, starch and sucrose metabolism, and TCA cycle; 5 (41.7%) amino metabolism-related pathways were amino acid biosynthesis, cysteine and methionine metabolism, tyrosine metabolism, glutathione metabolism, and arginine biosynthesis; and 1 nucleotide anabolism-related pathway was purine metabolism.

The 12 significantly upregulated pathways were mainly associated with bacterial resistance. The upregulation of two-component system and PTS in the environmental information processing pathway increased biological transshipment, regulation, signal transduction, and external stimulus response in *bacteria* after injury, decreasing the entry of AMPs into the bacteria.[41] Meanwhile, the upregulation of the cellular process pathways of flagellar components, peptidoglycan biosynthesis, and O-antigenic nucleotide sugar biosynthesis allows the bacteria to move away from high concentrations of AMPs via chemotaxis.[42] Additionally, the upregulation of fructose and mannose metabolism and amino sugar and nucleotide sugar metabolism enables the bacteria to use energy metabolic branches for the energy supply when normal energy metabolic pathways are inhibited. The upregulation of CAMP resistance indicates bacterial resistance to antimicrobial agents.[43] Furthermore, the upregulation of metabolic pathways of selenium complex metabolism, sulfur metabolism, and protein export was due to the antimicrobial peptide-mediated disruption of the cell membrane, leading to the efflux of intracellular substances.

The five lowest p-value significantly enriched metabolic pathways (pyruvate metabolism, amino acid biosynthesis, purine metabolism, carbon metabolism, and glycolysis/gluconeogenesis) were selected. The differential proteins in these pathways were plotted for network construction. As shown in Figure 5H, the carbon metabolism pathway was at the center of the pathway/protein interaction graph and was connected to the other four pathways. The proteins that connect the different pathways were all enzymes. It is worth noting that carbamate kinase (A0A0D6HNW0), as the second lowest FDR protein, linked the carbon metabolism pathway and purine metabolism pathway. In addition, 2,3-diphosphoglycerate-dependent phosphoglycerate mutase (dPGM) (Q8ZQS2) linked more pathways.

3.4. Correlation between Metabolomic and Proteomic Analysis Results. As shown in Figure 6A, the differential metabolites and differential proteins were involved in 105 KEGG pathways. Of these, 68 pathways were detected simultaneously in metabolomic and proteomic analyses, while 7 and 30 pathways were uniquely detected in metabolomic and proteomic analyses, respectively. This is consistent with the results of Mironenka et al.[23] who used the combination of metabolomics and proteomics to examine the effect of *Trichoderma* metabolites on *Fusarium* metabolism. The plausible rationale behind this consistency could be attributed to a higher count of proteins annotated in the KEGG pathway compared with that of metabolites.

The shared pathways of the metabolome and proteome were analyzed jointly (Figure 6B). The effect of JHBp2 on *S. typhimurium* metabolism covered 10 classes out of a total of 13 classes of secondary metabolic pathways. In the global maps, 352 differential proteins and metabolites were involved in metabolic pathways, 145 were involved in the biosynthesis of secondary metabolites, and 108 were involved in microbial metabolism in different environments. In the overview maps, amino acid biosynthesis, carbon metabolism, and fatty acid metabolism had 65, 61, and 12 differential proteins and metabolites, respectively.

Among the pathways involving specific classes of metabolites, pyruvate, amino acid, and nucleotide metabolism correspond to the carbohydrate metabolic pathway; purine and pyrimidine metabolism correspond to the nucleotide metabolic pathway; alanine, aspartate, and glutamate metabolism correspond to the amino acid metabolic pathway; porphyrin metabolism was as the biosynthesis of cofactors, and all involved more than 20 differential proteins or metabolites.

The impact of JHBp2 on the metabolism of *Salmonella typhimurium* mainly centered on energy metabolism, nucleotide synthesis metabolism, and amino acid synthesis metabolism. Based on the p-value heatmap showing the shared KEGG pathway of the metabolome and proteome (Figure 6C), purine metabolism, glutathione metabolism, biosynthesis of cofactors, pyrimidine metabolism, carbon metabolism, pyruvate metabolism, amino acid biosynthesis, and TCA cycle-related metabo-

https://doi.org/10.1021/acs.jafc.4c01531
J. Agric. Food Chem. 2024, 72, 14433−14447

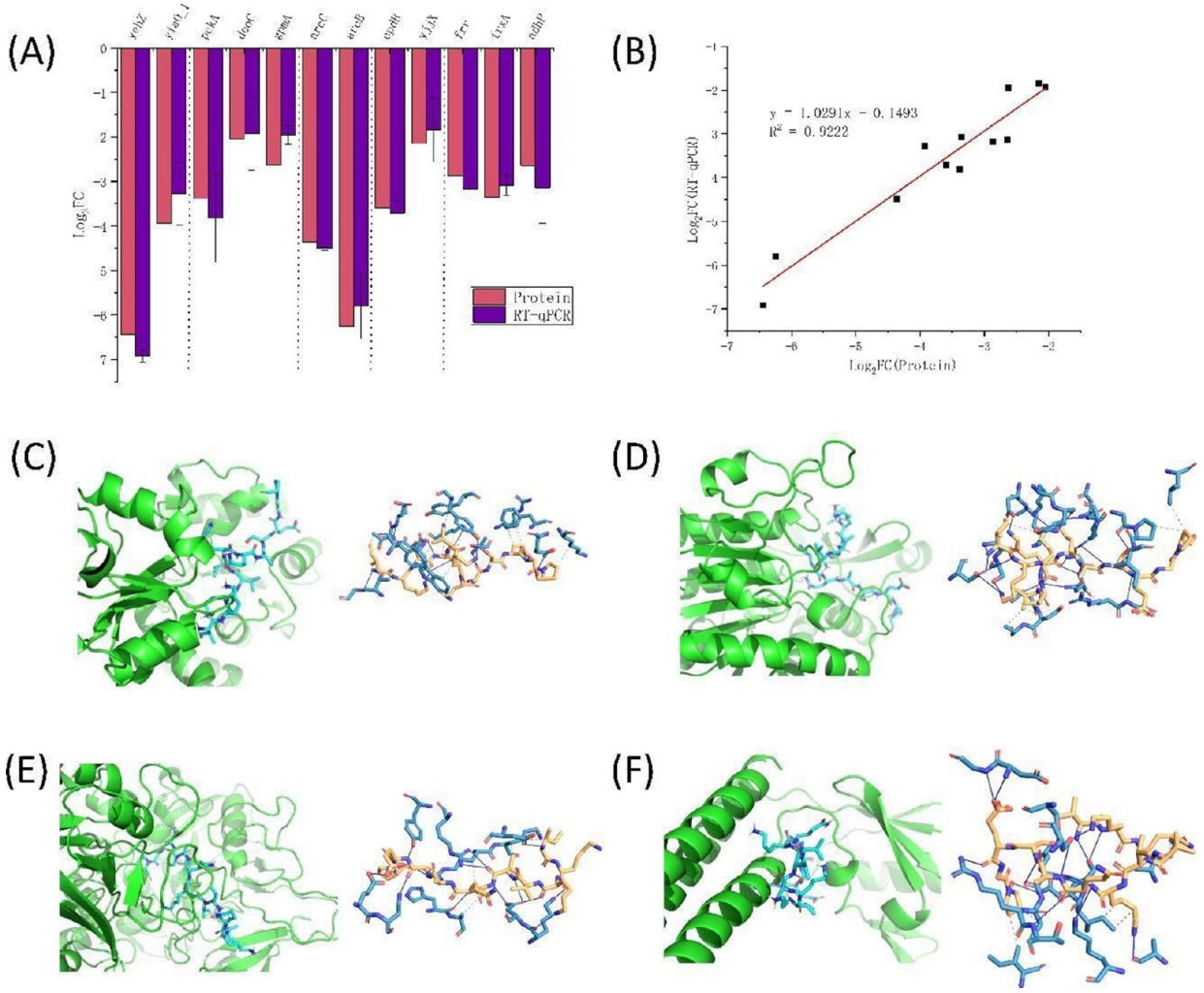

Figure 7. Real-time qPCR and molecular docking. (A) RT-qPCR detection of gene expression. (B) Correlation analysis between proteomic results and RT-qPCR results. Best ranked docking orientations for (C) YehZ, (D) ArcC, (E) CpdB, and (F) frr binding with JHBp2.

lites and proteins were significantly different in the metabolome and proteome.

Multiple pathways of energy metabolism, amino acid synthesis metabolism, and nucleotide metabolism were connected by the carbon metabolism pathway. Further analysis of the differential metabolites and differential proteins involved in carbon metabolism could aid in elucidating the molecular mechanisms underlying the effects of JHBp2 on bacteria. As shown in Figure 6D, among the differential metabolites involved in carbon metabolism, NAD(P)+, NADH, succinate, fumarate, D-Erythrose-4-phosphate, phosphate, CoA, and acetyl-CoA were involved in energy metabolic pathways; ADP, UDP, and AMP were involved in nucleotide synthesis and metabolism; and O-phosphate-L-serine and L-glutamate were involved in amino acid synthesis and metabolism.

2,3-Bisphosphoglycerate-dependent phosphoglycerate mutase (dPGM), transaldolase A, and transaldolase B exhibit direct interactions. Fumarate hydratase II directly interacts with malate dehydrogenase. PGM is an important enzyme family for energy metabolism, connecting multiple energy metabolic pathways.[44] PGM occupies an important position in the network. The downregulation of PGM can significantly suppress metabolic pathways, such as glycolysis and TCA cycle.[45] Among the other differential proteins, acetyl coenzyme A synthase was involved in energy metabolic pathways, phosphoserine aminotransferase and cysteine synthase B were involved in amino acid synthesis and metabolism, and ribulose-5-phosphate isomerase A was involved in nucleotide synthesis and metabolism. The alpha subunit of the fatty acid oxidation complex was also a differential protein.

3.5. RT-qPCR Validation. The five proteins with the lowest FDR values in the transmembrane transport, carbon metabolism, amino acid biosynthesis/metabolism, and nucleotide metabolism pathway are listed in Table S6. The transmembrane transport (yehZ, yiaO_1), carbon metabolism (pckA, deoC, gpmA), amino acid biosynthesis/metabolism (arcC, arcB), nucleotide metabolism (cpdB, yjjX), and some other lowest FDR proteins (frr, trxA, adhP), totaling 12 proteins, were selected for RT-qPCR validation of relevant mRNA expression. As shown in Figure 7A, the mRNA expression associated with the 12 selected proteins was all downregulated, which is consistent with the trend of the proteomic results. Meanwhile, correlation analysis of proteomics and RT-qPCR results (Figure 7B) showed a positive correlation. All of the above data indicated that the proteomic results were reliable.

3.6. Molecular Docking of JHBp2 toward Differentially Expressed Protein. When the binding energy is ≤−7 kcal/mol, it can be assumed that the protein and ligand can bind

https://doi.org/10.1021/acs.jafc.4c01531
J. Agric. Food Chem. 2024, 72, 14433−14447

stably.[46] As shown in Table 1, the binding energy of ArcC (−8.1), YehZ (−7.4), CpdB (−7.0), and frr (−7.0) was ≤−7 kcal/mol, and thus, JHBp2 could bind stably to these four proteins. ArcC (Carbamate Kinase), YehZ (ABC Transporter Substrate-Binding Protein), and CpdB (2′,3′-Cyclic-Nucleotide-2′-Phosphodiesterase/3′-Nucleotidase) are involved in transmembrane transport, amino acid biosynthesis/metabolism, and nucleotide metabolism, respectively. Frr (Ribosome-Recycling Factor) is the differentially expressed protein with the lowest FDR value, except for Duf2511 domain-containing protein and carbamate kinase. As shown in Table S7, These 4 proteins formed at least 13 hydrogen bonds with JHBp2, which is more than the other 8 proteins. The binding energy of ArcC (Carbamate Kinase) and JHBP2 is the lowest and thus more stable, owing to the fact that ArcC can form 23 hydrogen bonds with JHBp2, which is the most among all the 12 proteins.

Table 1. Binding Energy of JHBP2 and Docking Proteins

gene name	protein name	affinity (kcal/mol)
ArcC	carbamate kinase	−8.1
YehZ	ABC transporter substrate-binding protein	−7.4
CpdB	2′,3′-cyclic-nucleotide 2′-phosphodiesterase/3′-nucleotidase	−7
Frr	ribosome-recycling factor	−7
YjjX	inosine/xanthosine triphosphatase	−6.4
AdhP	alcohol dehydrogenase	−6.3
TrxA	thioredoxin 1	−6.2
GpmA	2,3-bisphosphoglycerate-dependent phosphoglycerate mutase	−5.9
ArcB	ornithine carbamoyltransferase	−5.6
PckA	phosphoenolpyruvate carboxykinase	−5.3
DeoC	deoxyribose-phosphate aldolase	−4.7
YiaO_1	C4-dicarboxylate Abc transporter substrate-binding protein	−4.6

After molecular docking visualization, it can be known that JHBp2 fell into the active pockets of YehZ (Figure 7C), ArcC (Figure 7D), CpdB (Figure 7E), and frr (Figure 7F) and stably bound to them through hydrogen bonding and hydrophobic interactions. In addition, Figure S1 showed the visualization of molecular docking between JHBp2 and the other 8 proteins.

4. DISCUSSION

Based on the integrated nucleic acid and protein leakage result and metabolomic and proteomic analysis, the growth inhibitory mechanisms of JHBp2 against *S. typhimurium* (Figure 8) could be summarized as follows:

1. **JHBp2 destroyed the structure of the cell membrane and interfered with bacterial cell membrane-associated protein synthesis, thus disrupted cell membrane function.** Liu et al.[47] performed transcriptomics analysis to demonstrate that *Xanthomonas* sp. growth was inhibited after phenazine treatment, the transmembrane transporter activity, DNA-mediated transposition, and structural molecular activity decreased. The scanning electron microscope indicates that the structure of bacterial cell walls and membranes was disrupted after JHBp2 treatment. Further, subcellular localization analysis revealed that more than 65% of the differential proteins in the AMPT group were localized to the cell membrane. KEGG analysis of the metabolome suggested that the levels of 14 metabolites involved in the ABC transporter pathway were significantly altered. Of these, 10 were significantly downregulated. YehZ (ABC Transporter Substrate-Binding Protein) expression was also significantly downregulated in RT-qPCR experiments. The ABC transporter, an important protein expressed on the bacterial cell membrane, actively transfers ligands to the cell membrane. Thus, the ABC transporter is related to bacterial resistance and has a role in secreting cytotoxic molecules.[48] The JHBp2-mediated downregulation of ABC transporter-related metabolites indicated that the important functions of *S. typhimurium* membrane structural proteins were inhibited, preventing the

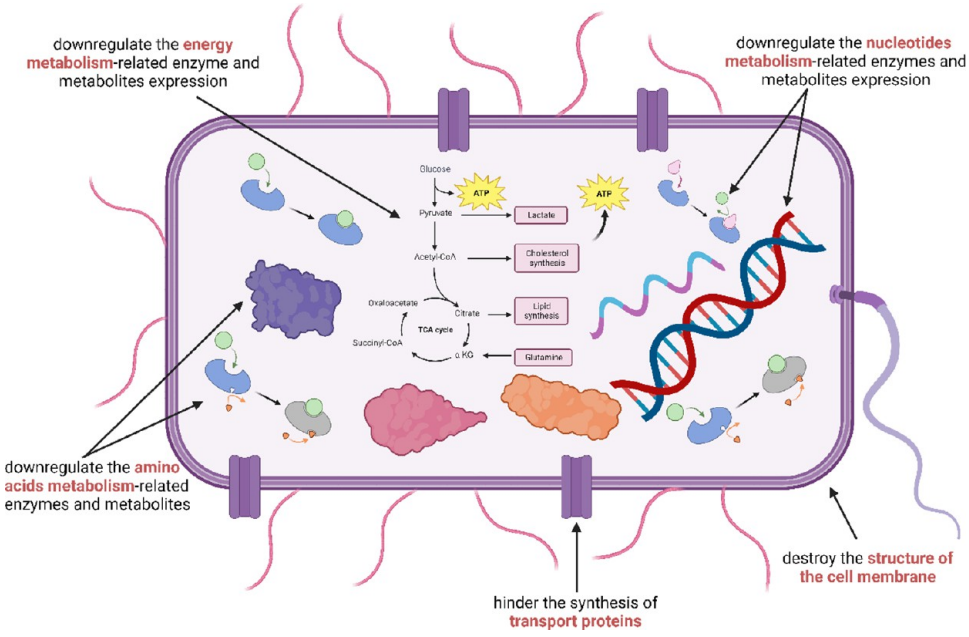

Figure 8. Mechanism of JHBp2 against *Salmonella typhimurium* in vitro.

https://doi.org/10.1021/acs.jafc.4c01531
J. Agric. Food Chem. 2024, 72, 14433−14447

development of drug resistance. Additionally, GO annotation analysis revealed a significant downregulation of proteins related to periplasmic space and outer membrane periplasmic space, which containing a large number of hydrolytic and synthetic enzymes associated with peptidoglycan synthesis, as well as binding proteins that aid in nutrient transport.[49] The significant downregulation of these proteins suppressed the nutrient uptake by bacteria.

2. **JHBp2 significantly downregulated energy metabolism-related enzyme and metabolites expression, which affected normal energy metabolism and cellular respiration in bacteria**. KEGG analysis of the proteome revealed that 6 of the 12 significantly downregulated pathways were involved in energy metabolism, including pyruvate metabolism, carbon metabolism, glycolysis/gluconeogenesis, dicarboxylic acid metabolism, starch and sucrose metabolism, and TCA cycle with pyruvate metabolism being the most significantly downregulated pathway. The differential metabolites including acetyl coenzyme A, ferredoxin, and succinate were involved in several metabolic pathways. The downregulation of these metabolites altered energy metabolism. The findings align with the observations of Zhao et al.,[50] which demonstrated that the combination of nisin and grape seed extract exerted growth inhibitory effects against *Listeria monocytogenes*. This effect was achieved through interference with the tricarboxylic acid (TCA) cycle, amino acid biosynthesis, and energy production pathways, contributing to the disruption of intracellular metabolism.

   In the network diagram of pathways and their related proteins, carbon metabolism was centrally located and connected to all other significant metabolic pathways. Of the five significant metabolic pathways, 2,3-diphosphoglycerate-dependent PGM (dPGM) linked four pathways. dPGM, an important enzyme family for ATP binding, has an important role in energy metabolism,[51] with its function contingent on the cofactor 2,3-diphosphoglycerate. Energy metabolism-related enzymes, such as fumarate hydratase II, malate dehydrogenase, fructose diphosphate aldolase, and acetyl coenzyme A synthase, were significantly downregulated in the AMPT group. Among the metabolomics, 24 differential metabolites were involved in the biosynthesis of cofactors pathway, which accounted for the highest number of differential metabolites among all pathways. Meanwhile, 18 differential proteins were involved in the biosynthesis of cofactors pathway in proteomics.

3. **JHBp2 significantly downregulated the synthesis/metabolism of amino acids, nucleotides-related enzymes, and metabolites, thereby interfering with normal genetic material and protein synthesis**. Differential metabolites of amino acids and nucleotide, such as glutamate and 5,6-Dihydrouracil, are important raw materials for protein and nucleic acid synthesis in *S. typhimurium*. Downregulation of amino acid and nucleotide expression can render the suppression of proteins and nucleic acids anabolism detrimental to the cells' physiological and biochemical responses. Remarkably, glutathione, a crucial component in scavenging cellular-free radicals, plays an important role in the antioxidant response of cells.[52] Moreover, nucleotides participated in the synthesis of DNA and RNA, which were involved in encoding bacterial genetic information and closely related to physiological processes such as transcription and translation. The suppression of nucleotide biosynthesis inhibits healthy cell division and differentiation.[53] Proteomic and RT-qPCR analysis revealed that structure-related enzymes associated with amino acid and nucleotide anabolism (such as carbamate cinase and 2′,3′-cyclic-nucleotide-2′-phosphodiesterase/3′-nucleotidase) were significantly downregulated upon the JHBp2 treatment. Molecular docking results also demonstrated that JHBp2 can bind stably to both enzymes. Metabolomic analysis underscored 10 differential metabolites related to glutathione metabolism, which were all downregulated in the AMPT group. Additionally, 15 and 10 differential metabolites were associated with purine metabolism and pyrimidine metabolism, respectively. Of these, 10 purine metabolism-related metabolites and 8 pyrimidine metabolism-related metabolites were downregulated in the AMPT group. Glutamate was significantly downregulated and was involved in six metabolism pathways in the AMPT group.

Consequently, JHBp2 destroyed the structure of the cell wall and membrane, inhibited the bacterial absorption of nutrients, affected normal energy metabolism, and interfered with regular genetic material and protein synthesis, thereby inhibiting bacterial growth.

■ ASSOCIATED CONTENT

Supporting Information

The Supporting Information is available free of charge at https://pubs.acs.org/doi/10.1021/acs.jafc.4c01531.

Best ranked docking orientations for YiaO_1, PckA, DeoC, GpmA, ArcB, YjjX, TrxA, and AdhP binding with JHBp2; msfragger parameter settings; sequences of primers of RT-qPCR; MIC of $JHBP_2$ against *S. typhimurium*; sample protein extraction amount; top 10 lowest FDR proteins; detailed information on differentially expressed proteins in some pathways; and chemical bonds of JHBP2 and docking proteins (PDF)

■ AUTHOR INFORMATION

Corresponding Author

Wangang Zhang − *Key Laboratory of Meat Processing and Quality Control, Ministry of Education China, Jiangsu Collaborative Innovation Center of Meat Production and Processing, Quality and Safety Control, College of Food Science and Technology, Nanjing Agricultural University, Nanjing 210095, China;* orcid.org/0000-0001-6910-130X; Phone: +86-25-84385341; Email: wangang.zhang@njau.edu.cn; Fax: +86-25-84395341

Authors

Ziyi Yang − *Key Laboratory of Meat Processing and Quality Control, Ministry of Education China, Jiangsu Collaborative Innovation Center of Meat Production and Processing, Quality and Safety Control, College of Food Science and Technology, Nanjing Agricultural University, Nanjing 210095, China*

Zixu Wang − *Key Laboratory of Meat Processing and Quality Control, Ministry of Education China, Jiangsu Collaborative Innovation Center of Meat Production and Processing, Quality*

and Safety Control, College of Food Science and Technology, Nanjing Agricultural University, Nanjing 210095, China

Ruoxin Wang − *Key Laboratory of Meat Processing and Quality Control, Ministry of Education China, Jiangsu Collaborative Innovation Center of Meat Production and Processing, Quality and Safety Control, College of Food Science and Technology, Nanjing Agricultural University, Nanjing 210095, China*

Complete contact information is available at: https://pubs.acs.org/10.1021/acs.jafc.4c01531

Funding

This work was financially supported by the earmarked fund for China Agriculture Research System (CARS-35).

Notes

The authors declare no competing financial interest.

■ ACKNOWLEDGMENTS

We thank Yixuan Xu and Jing Li for their help in revising the grammar of this paper. We thank Fajian Li at Shanghai Bioprofile Technology Company Ltd. for his technical support.

■ REFERENCES

(1) Delahoy, M. J.; Shah, H. J.; Weller, D. L.; Ray, L. C.; Smith, K.; Mcguire, S.; Trevejo, R. T.; Walter, E. S.; Wymore, K.; Rissman, T. Preliminary incidence and trends of infections caused by pathogens transmitted commonly through food-foodborne diseases active surveillance network, 10 us sites, 2022. *Morb. Mortal. Wkly. Rep.* **2023**, *72* (26), 701−706.

(2) Klemm, E. J.; Shakoor, S.; Page, A. J.; Qamar, F. N.; Judge, K.; Saeed, D. K.; Wong, V. K.; Dallman, T. J.; Nair, S.; Baker, S.; et al. Emergence of an extensively drug-resistant salmonella enterica serovar typhi clone harboring a promiscuous plasmid encoding resistance to fluoroquinolones and third-generation cephalosporins. *mBio* **2018**, *9*, No. e00105-81.

(3) Tamma, P. D.; Avdic, E.; Li, D. X.; Dzintars, K.; Cosgrove, S. E. Association of adverse events with antibiotic use in hospitalized patients. *JAMA Int. Med.* **2017**, *177* (9), 1308−1315.

(4) Li, S.; Wang, Y.; Xue, Z.; Jia, Y.; Li, R.; He, C.; Chen, H. The structure-mechanism relationship and mode of actions of antimicrobial peptides: a review. *Trends Food Sci. Technol.* **2021**, *109*, 103−115.

(5) Tan, P.; Fu, H.; Ma, X. Design, optimization, and nanotechnology of antimicrobial peptides: from exploration to applications. *Nano Today* **2021**, *39*, No. 101229.

(6) Chai, T.; Tan, Y.; Ee, K.; Xiao, J.; Wong, F. Seeds, fermented foods, and agricultural by-products as sources of plant-derived antibacterial peptides. *Crit. Rev. Food Sci. Nutr.* **2019**, *591* (SI), S162−S177.

(7) Xing, L.; Liu, R.; Cao, S.; Zhang, W.; Zhou, G. Meat protein based bioactive peptides and their potential functional activity: a review. *Int. J. Food Sci. Technol.* **2019**, *54* (6SI), 1956−1966.

(8) Kurnaz, L. B.; Luo, Y.; Yang, X.; Alabresm, A.; Leighton, R.; Kumar, R.; Hwang, J.; Decho, A. W.; Nagarkatti, P.; Nagarkatti, M. Facial amphiphilicity index correlating chemical structures with antimicrobial efficacy. *Bioact. Mater.* **2023**, *20*, 519−527.

(9) Lin, T.; Weibel, D. B. Organization and function of anionic phospholipids in bacteria. *Appl. Microbiol. Biotechnol.* **2016**, *100* (10), 4255−4267.

(10) Zhu, X.; Shan, A.; Ma, Z.; Xu, W.; Wang, J.; Chou, S.; Cheng, B. Bactericidal efficiency and modes of action of the novel antimicrobial peptide t9w against pseudomonas aeruginosa. *Antimicrob. Agents Chemother.* **2015**, *59* (6), 3008−3017.

(11) Nguyen, L. T.; Haney, E. F.; Vogel, H. J. The expanding scope of antimicrobial peptide structures and their modes of action. *Trends Biotechnol.* **2011**, *29* (9), 464−472.

(12) Conte, M.; Aliberti, F.; Fucci, L.; Piscopo, M. Antimicrobial activity of various cationic molecules on foodborne pathogens. *World J. Microbiol. Biotechnol.* **2007**, *23* (12), 1679−1683.

(13) Zhou, B.; Shen, Z.; Liu, Y.; Wang, C.; Shen, Q. W. Proteomic analysis reveals that lysine acetylation mediates the effect of antemortem stress on postmortem meat quality development. *Food Chem.* **2019**, *293*, 396−407.

(14) Zhang, J.; Zhen, Z.; Zhang, W.; Zeng, T.; Zhou, G. Effect of intensifying high-temperature ripening on proteolysis, lipolysis and flavor of jinhua ham. *J. Sci. Food Agric.* **2009**, *89* (5), 834−842.

(15) Xing, L.; Liu, R.; Gao, X.; Zheng, J.; Wang, C.; Zhou, G.; Zhang, W. The proteomics homology of antioxidant peptides extracted from dry-cured xuanwei and jinhua ham. *Food Chem.* **2018**, *266*, 420−426.

(16) Xing, L.; Fu, L.; Hao, Y.; Miao, Y.; Zhang, W. Xuanwei ham derived peptides exert the anti-inflammatory effect in the dextran sulfate sodium-induced c57bl/6 mice model. *Food Biosci.* **2022**, *48*, No. 101800.

(17) Castellano, P.; Mora, L.; Escudero, E.; Vignolo, G.; Aznar, R.; Toldra, F. Antilisterial peptides from spanish dry-cured hams: purification and identification. *Food Microbiol.* **2016**, *59*, 133−141.

(18) Yang, Z.; Cai, J.; Boateng, E. F.; Xing, L.; Zhang, W. Insight into antioxidant activity and peptide profile of jinhua ham broth peptides at different cooking times. *Antioxidants* **2023**, *12* (6063). DOI: 606.

(19) Mei, L.; Zhu, S.; Liu, Y.; Yin, W.; Gu, Z.; Zhao, Y. An overview of the use of nanozymes in antibacterial applications. *Chem. Eng. J.* **2021**, *418*, No. 129431.

(20) Lia, S.; Zhang, Y.; Pan, X.; Zhu, F.; Jiang, C.; Liu, Q.; Cheng, Z.; Dai, G.; Wu, G.; Wang, L.; et al. Antibacterial activity and mechanism of silver nanoparticles against multidrug-resistant pseudomonas aeruginosa. *Int. J. Nanomed.* **2019**, *14*, 1469−1487.

(21) Chen, L.; Zhao, X.; Li, R.; Yang, H. Integrated metabolomics and transcriptomics reveal the adaptive responses of salmonella enterica serovar typhimurium to thyme and cinnamon oils. *Food Res. Int.* **2022**, *157*, No. 111241.

(22) Du, H.; Zhou, L.; Lu, Z.; Bie, X.; Zhao, H.; Niu, Y. D.; Lu, F. Transcriptomic and proteomic profiling response of methicillin-resistant staphylococcus aureus (mrsa) to a novel bacteriocin, plantaricin gz1−27 and its inhibition of biofilm formation. *Appl. Microbiol. Biotechnol.* **2020**, *104* (18), 7957−7970.

(23) Mironenka, J.; Rozalska, S.; Sobon, A.; Bernat, P. Trichoderma harzianum metabolites disturb fusarium culmorum metabolism: metabolomic and proteomic studies. *Microbiol. Res.* **2021**, *249*, No. 126770.

(24) Ikeda, N. Y.; Ambrosio, C. M. S.; Claudio Miano, A.; Rosalen, P. L.; Gloria, E. M.; Alencar, S. M. Essential oils extracted from organic propolis residues: an exploratory analysis of their antibacterial and antioxidant properties and volatile profile. *Molecules* **2021**, *26*, 4694.

(25) Hou, L.; Shi, Y.; Zhai, P.; Le, G. Inhibition of foodborne pathogens from the larvae of the by hf-1, a novel antibacterial peptide housefly (*musca domestica*) in medium and orange juice. *Food Control* **2007**, *18* (11), 1350−1357.

(26) Yang, S.; Yusoff, K.; Ajat, M.; Yap, W.; Lim, S. E.; Lai, K. Antimicrobial activity and mode of action of terpene linalyl anthranilate against carbapenemase-producing klebsiella pneumoniae. *J. Pharm. Anal.* **2021**, *11* (2), 210−219.

(27) Casciaro, B.; Cappiello, F.; Verrusio, W.; Cacciafesta, M.; Mangoni, M. L. Antimicrobial peptides and their multiple effects at sub-inhibitory concentrations. *Curr. Top. Med. Chem.* **2020**, *20* (14), 1264−1273.

(28) Cheng, Q.; Zhang, J.; Fang, J.; Ding, H.; Xu, Y.; Lu, X.; Zhang, W. Untargeted metabolomics reveals the role of aqp9 in nonalcoholic fatty liver disease in a mice model. *Int. J. Biol. Macromol.* **2022**, *219*, 864−875.

(29) Glatter, T.; Ahrne, E.; Schmidt, A. Comparison of different sample preparation protocols reveals lysis buffer-specific extraction biases in gram-negative bacteria and human cells. *J. Proteome Res.* **2015**, *14* (11), 4472−4485.

(30) Yu, F.; Teo, G. C.; Kong, A. T.; Haynes, S. E.; Avtonomov, D. M.; Geiszler, D. J.; Nesvizhskii, A. I. Identification of modified peptides using localization-aware open search. *Nat. Commun.* **2020**, *11*, 40651.

(31) Kong, A. T.; Leprevost, F. V.; Avtonomov, D. M.; Mellacheruvu, D.; Nesvizhskii, A. I. Msfragger: ultrafast and comprehensive peptide

identification in mass spectrometry-based proteomics. *Nat. Methods* **2017**, *14* (5), 513.
(32) Riniker, S.; Landrum, G. A. Better informed distance geometry: using what we know to improve conformation generation. *J. Chem. Inf. Model.* **2015**, *55* (12), 2562−2574.
(33) Friedrich, N.; Meyder, A.; Kops, C. D. B.; Sommer, K.; Flachsenberg, F.; Rarey, M.; Kirchmair, J. High-quality dataset of protein-bound ligand conformations and its application to benchmarking conformer ensemble generators. *J. Chem. Inf. Model.* **2017**, *57* (3), 529−539.
(34) Halgren, T. A.; Nachbar, R. B. Merck molecular force field. 4. Conformational energies and geometries for mmff94. *J. Comput. Chem.* **1996**, *17* (5−6), 587−615.
(35) Masters, L.; Eagon, S.; Heying, M. Evaluation of consensus scoring methods for autodock vina, smina and idock. *J. Mol. Graph.* **2020**, *96*, No. 107532.
(36) Mooers, B. H. M. Shortcuts for faster image creation in pymol. *Protein Sci.* **2020**, *29* (1SI), 268−276.
(37) Adasme, M. F.; Linnemann, K. L.; Bolz, S. N.; Kaiser, F.; Salentin, S.; Haupt, V. J.; Schroeder, M. Plip 2021: expanding the scope of the protein-ligand interaction profiler to dna and rna. *Nucleic Acids Res.* **2021**, *49* (W1), W530−W534.
(38) van der Mei, H. C.; van de Belt-Gritter, B.; Pouwels, P. H.; Martinez, B.; Busscher, H. J. Cell surface hydrophobicity is conveyed by s-layer proteins - a study in recombinant lactobacilli. *Colloid Surf., B* **2003**, *28*, 127−134.
(39) Zhang, Z.; Jiang, B.; Liao, X.; Yi, J.; Hu, X.; Zhang, Y. Inactivation of bacillus subtilis spores by combining high-pressure thermal sterilization and ethanol. *Int. J. Food Microbiol.* **2012**, *160* (2), 99−104.
(40) Dezi, M.; Di Cicco, A.; Bassereau, P.; Levy, D. Detergent-mediated incorporation of transmembrane proteins in giant unilamellar vesicles with controlled physiological contents. *Proc. Natl. Acad. Sci. U. S. A.* **2013**, *110* (18), 7276−7281.
(41) Luettmann, D.; Goepel, Y.; Goerke, B. The phosphotransferase protein eiiantr modulates the phosphate starvation response through interaction with histidine kinase phor in escherichia coli. *Mol. Microbiol.* **2012**, *86* (1), 96−110.
(42) Gottesman, S.; Harwood, C. S.; Lertsethtakarn, P.; Ottemann, K. M.; Hendrixson, D. R. Motility and chemotaxis in campylobacter and helicobacter. *Annu. Rev. Microbiol.* **2011**, *65*, 389−410.
(43) Shafer, W. M.; Kraus, D.; Peschel, A. Molecular mechanisms of bacterial resistance to antimicrobial peptides. *Curr. Top. Microbiol. Immunol.* **2006**, *306*, 231−250.
(44) Kumar, A.; Rai, L. C. Proteomic and biochemical basis for enhanced growth yield of enterobacter sp lcr1 on insoluble phosphate medium. *Microbiol. Res.* **2015**, *170*, 195−204.
(45) Smith, A.; Mccann, M.; Kavanagh, K. Proteomic analysis of the proteins released from staphylococcus aureus following exposure to ag(i). *Toxicol. Vitro* **2013**, *27* (6), 1644−1648.
(46) Cui, Z.; Zhang, N.; Zhou, T.; Zhou, X.; Meng, H.; Yu, Y.; Zhang, Z.; Zhang, Y.; Wang, W.; Liu, Y. Conserved sites and recognition mechanisms of t1r1 and t2r14 receptors revealed by ensemble docking and molecular descriptors and fingerprints combined with machine learning. *J. Agric. Food Chem.* **2023**, *71* (14), 5630−5645.
(47) Liu, Q.; Yang, J.; Ahmed, W.; Wan, X.; Wei, L.; Ji, G. Exploiting the antibacterial mechanism of phenazine substances from lysobacter antibioticus 13−6 against xanthomonas oryzae pv. Oryzicola. *J. Microbiol.* **2022**, *60* (5), 496−510.
(48) Linton, K. J. Structure and function of abc transporters. *Physiology* **2007**, *22*, 122−130.
(49) Stock, J. B.; Rauch, B.; Roseman, S. Periplasmic space in salmonella typhimurium and escherichia coli. *J. Biol. Chem.* **1977**, *252* (21), 7850−7861.
(50) Zhao, X.; Chen, L.; Wu, J.; He, Y.; Yang, H. Elucidating antimicrobial mechanism of nisin and grape seed extract against listeria monocytogenes in broth and on shrimp through nmr-based metabolomics approach. *Int. J. Food Microbiol.* **2020**, *319*, No. 108494.
(51) Leyvavazquez, M. A.; Setlow, P. Cloning and nucleotide-sequences of the genes encoding triose phosphate isomerase, phosphoglycerate mutase, and enolase from bacillus-subtilis. *J. Bacteriol.* **1994**, *176* (13), 3903−3910.
(52) Noctor, G.; Arisi, A.; Jouanin, L.; Valadier, M. H.; Roux, Y.; Foyer, C. H. Light-dependent modulation of foliar glutathione synthesis and associated amino acid metabolism in poplar over-expressing gamma-glutamylcysteine synthetase. *Planta* **1997**, *202* (3), 357−369.
(53) Setlow, P. Deoxyribonucleic acid synthesis and deoxynucleotide metabolism during bacterial spore germination. *J. Bacteriol.* **1973**, *114* (3), 1099−1107.

https://doi.org/10.1021/acs.jafc.4c01531
J. Agric. Food Chem. 2024, 72, 14433−14447